9

Astronomical Tide and Typhoon-Induced Storm Surge in Hangzhou Bay, China

Jisheng Zhang[1], Chi Zhang[1], Xiuguang Wu[2] and Yakun Guo[3]

[1]*State Key Laboratory of Hydrology-Water Resources and Hydraulic Engineering, Hohai University, Nanjing, 210098*

[2]*Zhejiang Institute of Hydraulics and Estuary, Hangzhou, 310020*

[3]*School of Engineering, University of Aberdeen, Aberdeen, AB24 3UE*

[1,2]*China*

[3]*United Kingdom*

1. Introduction

The Hangzhou Bay, located at the East of China, is widely known for having one of the world's largest tidal bores. It is connected with the Qiantang River and the Eastern China Sea, and contains lots of small islands collectively referred as Zhoushan Islands (see Figure 1). The estuary mouth of the Hangzhou Bay is about 100 km wide; however, the head of bay (Ganpu) which is 86 km away from estuary mouth is significantly narrowed to only 21 km wide. The tide in the Hangzhou Bay is an anomalistic semidiurnal tide due to the irregular geometrical shape and shallow depth and is mainly controlled by the M_2 harmonic constituent. The M_2 tidal constituent has a period about 12 hours and 25.2 minutes, exactly half a tidal lunar day. The Hangzhou Bay faces frequent threats from tropical cyclones and suffers a massive damage from its resulting strong wind, storm surge and inland flooding. According to the 1949-2008 statistics, about 3.5 typhoons occur in this area every year. When typhoon generated in tropic open sea moves towards the estuary mouth, lower atmospheric pressure in the typhoon center causes a relatively high water elevation in adjacent area and strong surface wind pushes huge volume of seawater into the estuary, making water elevation in the Hangzhou Bay significantly increase. As a result, the typhoon-induced external forces (wind stress and pressure deficit) above sea surface make the tidal hydrodynamics in the Hangzhou Bay further complicated.

In the recent years, some researches have been done to study the tidal hydrodynamics in the Hangzhou Bay and its adjacent areas. For example, Hu et al. (2000) simulated the current field in the Hangzhou Bay based on a 2D model, and their simulated surface elevation and current field preferably compared with the field observations. Su et al. (2001), Pan et al. (2007) and Wang (2009) numerically investigate the formulation, propagation and dissipation of the tidal bore at the head of Hangzhou Bay. Also, Cao & Zhu (2000), Xie et al. (2007), Hu et al. (2007) and Guo et al. (2009) performed numerical simulation to study the typhoon-induced

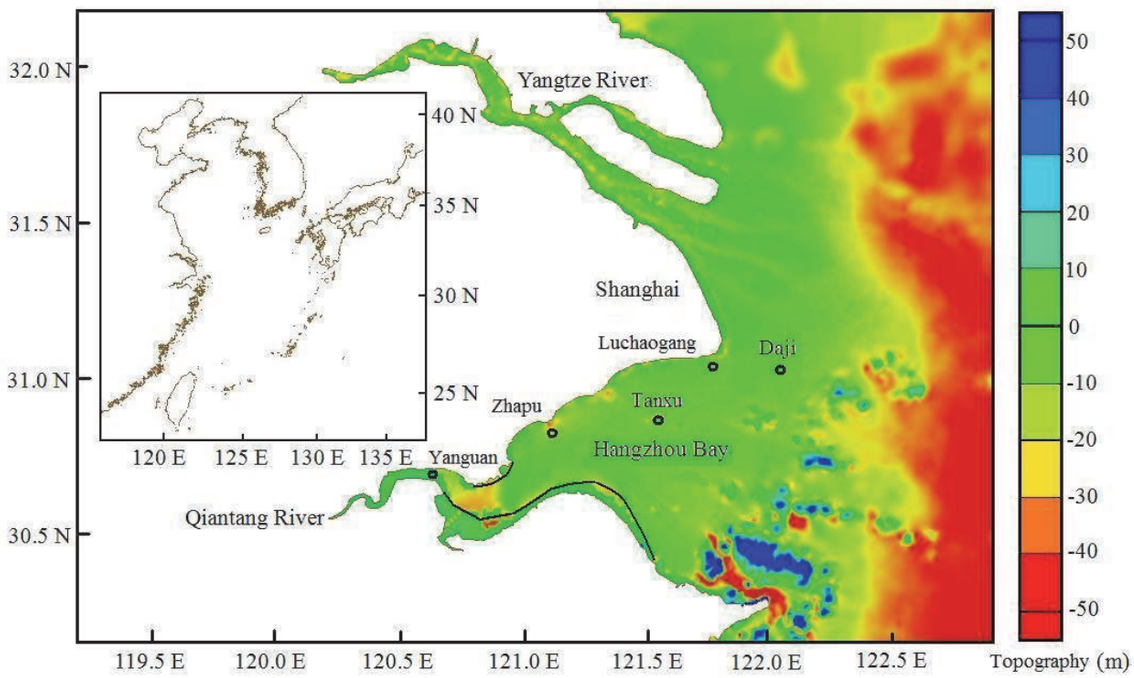

Fig. 1. Global location and 2005's bathymetry of the Hangzhou Bay and its adjacent shelf region

storm surge. However, most of them mainly focused on the 2D mathematical model. The main objective of this study is to understand the characteristics of (i) astronomical tide and (ii) typhoon-induced storm surge in the Hangzhou Bay based on the field observation and 3D numerical simulation.

2. Field observation

To understand the astronomical tides in the Hangzhou Bay, a five-month in situ measurement was carried out by the Zhejiang Institute of Hydraulic and Estuary from 01 April 2005 to 31 August 2005. There were eight fixed stations (T1-T8) along the banks of the Hangzhou Bay, at which long-term tidal elevations were measured every 30 minutes using ship-mounted WSH meter with the accuracy of ± 0.03 m. The tidal current velocity was recorded every 30 minutes at four stations H1-H4 using SLC9-2 meter, manufactured by Qiandao Guoke Ocean Environment and Technology Ltd, with precisions of $\pm 4^\circ$ in direction and $\pm 1.5\%$ in magnitude. The topography investigation in the Hangzhou Bay was also carried out in the early April 2005. Figure 2 shows the tidal gauge positions and velocity measurement points, together with the measured topography using different colors.

On 27/08/1981, a tropical depression named Agnes was initially formed about 600 km west-northwest of Guam in the early morning and it rapidly developed as a tropical storm moving west-northwestward (towards to Zhejiang Province) in the evening. Agnes became a typhoon in the morning of 29/08/1981, 165 km southwest of Okinawa next day. Agnes started to weaken after entering a region of hostile northerly vertical wind shear. The cyclonic center was almost completely disappeared by the morning of 02/09/1981. During Typhoon Agnes

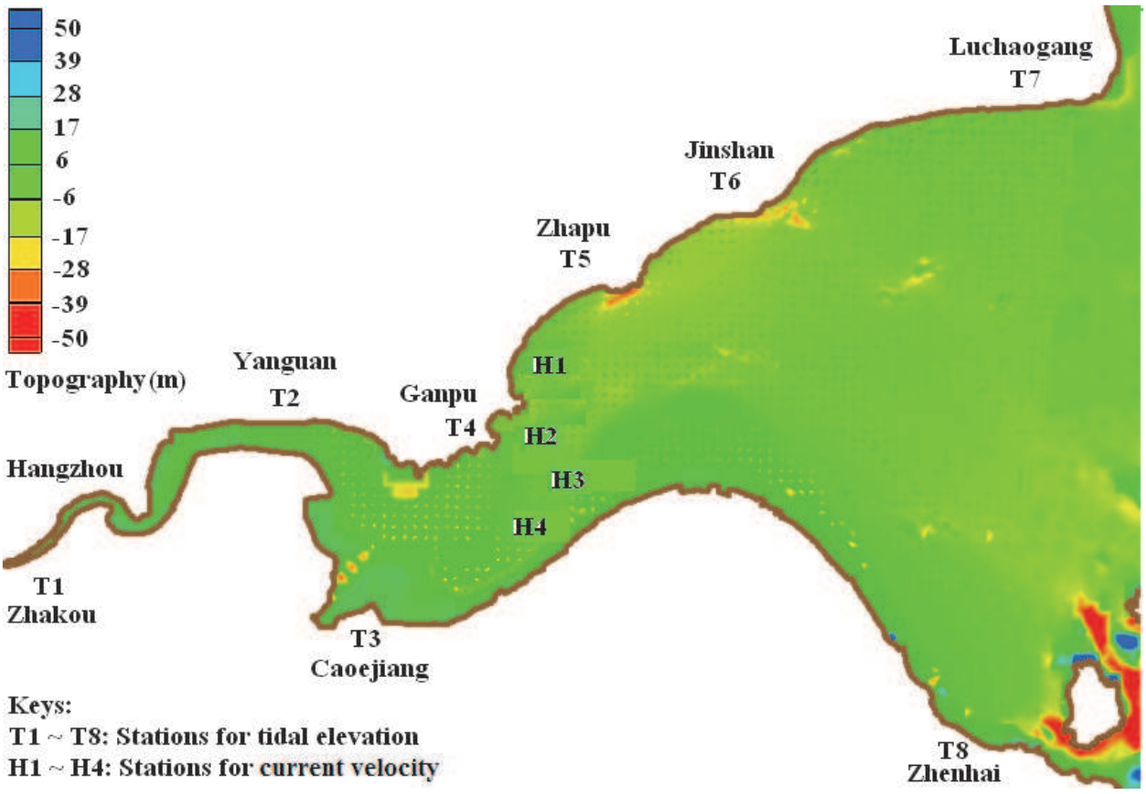

Fig. 2. A sketch of measurement stations and topography

(No.8114), which resulted in one of extremely recorded high water levels in the Hangzhou Bay, wind fields were observed every hour and storm tides were recorded every three hours at Daji station and Tanxu station (see Figure 1). Only the surge elevations were recorded and no current velocity was measured.

3. Numerical simulation

3.1 Governing equations

A 3D mathematical model based on FVCOM (an unstructured grid, Finite-Volume Coastal Ocean Model) (Chen et al., 2003) is developed for this study. The model uses an unstructured triangular grid in horizontal plane and a terrain-following σ-coordinate in vertical plane (see Figure 3), having a great ability to capture irregular shoreline and uneven seabed. The most sophisticated turbulence closure sub-model, Mellor-Yamada 2.5 turbulence model (Mellor & Yamada, 1982), is applied to compute the vertical mixing coefficients. More details of FVCOM can be found in Chen et al. (2003). Only the governing equations of the model are given here for completeness and convenience.

$$\frac{\partial \zeta}{\partial t} + \frac{\partial Du}{\partial x} + \frac{\partial Dv}{\partial y} + \frac{\partial \omega}{\partial \sigma} = 0 \tag{1}$$

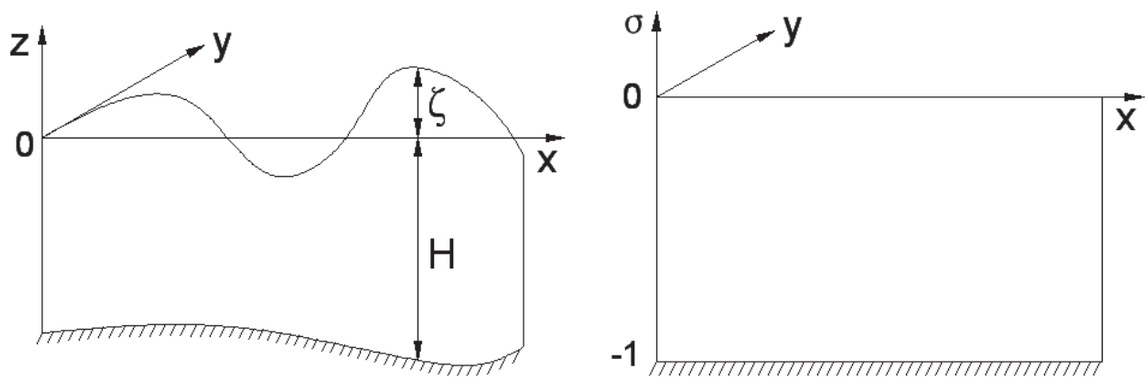

Fig. 3. Coordinate transformation of the vertical computational domain. Left: z-coordinate system; Right: σ-coordinate system

$$\frac{\partial uD}{\partial t}+\frac{\partial u^2D}{\partial x}+\frac{\partial uvD}{\partial y}+\frac{\partial u\omega}{\partial \sigma}=fvD-\frac{D}{\rho_o}\frac{\partial P_{atm}}{\partial x}-gD\frac{\partial \zeta}{\partial x} \\ -\frac{gD}{\rho_o}[\frac{\partial}{\partial x}(D\int_{\sigma}^{0}\rho d\sigma')+\sigma\rho\frac{\partial D}{\partial x}]+\frac{\partial}{\partial \sigma}(\frac{K_m}{D}\frac{\partial u}{\partial \sigma})+DF_u \tag{2}$$

$$\frac{\partial vD}{\partial t}+\frac{\partial uvD}{\partial x}+\frac{\partial v^2D}{\partial y}+\frac{\partial v\omega}{\partial \sigma}=-fuD-\frac{D}{\rho_o}\frac{\partial P_{atm}}{\partial y}-gD\frac{\partial \zeta}{\partial y} \\ -\frac{gD}{\rho_o}[\frac{\partial}{\partial y}(D\int_{\sigma}^{0}\rho d\sigma')+\sigma\rho\frac{\partial D}{\partial y}]+\frac{\partial}{\partial \sigma}(\frac{K_m}{D}\frac{\partial v}{\partial \sigma})+DF_v \tag{3}$$

$$\frac{\partial TD}{\partial t}+\frac{\partial TuD}{\partial x}+\frac{\partial TvD}{\partial y}+\frac{\partial T\omega}{\partial \sigma}=\frac{\partial}{\partial \sigma}(\frac{K_h}{D}\frac{\partial T}{\partial \sigma})+DF_T \tag{4}$$

$$\frac{\partial SD}{\partial t}+\frac{\partial SuD}{\partial x}+\frac{\partial SvD}{\partial y}+\frac{\partial S\omega}{\partial \sigma}=\frac{\partial}{\partial \sigma}(\frac{K_h}{D}\frac{\partial S}{\partial \sigma})+DF_S \tag{5}$$

$$\rho=\rho(T,S) \tag{6}$$

$$\frac{\partial q^2D}{\partial t}+\frac{\partial uq^2D}{\partial x}+\frac{\partial vq^2D}{\partial y}+\frac{\partial \omega q^2}{\partial \sigma}=\frac{2K_m}{D}[(\frac{\partial u}{\partial \sigma})^2+(\frac{\partial v}{\partial \sigma})^2]+\frac{2g}{\rho_o}K_h\frac{\partial \rho}{\partial \sigma} \\ -\frac{2Dq^3}{B_1 l}+\frac{\partial}{\partial \sigma}(\frac{K_{q^2}}{D}\frac{\partial q^2}{\partial \sigma})+DF_{q^2} \tag{7}$$

$$\frac{\partial q^2lD}{\partial t}+\frac{\partial uq^2lD}{\partial x}+\frac{\partial vq^2lD}{\partial y}+\frac{\partial \omega q^2l}{\partial \sigma}=\frac{lE_1K_m}{D}[(\frac{\partial u}{\partial \sigma})^2+(\frac{\partial v}{\partial \sigma})^2]+\frac{lE_1g}{\rho_o}K_h\frac{\partial \rho}{\partial \sigma} \\ -\frac{Dq^3}{B_1}\widetilde{W}+\frac{\partial}{\partial \sigma}(\frac{K_{q^2}}{D}\frac{\partial q^2l}{\partial \sigma})+DF_{q^2l} \tag{8}$$

where x, y and σ are the east, north and upward axes of the σ-coordinate system; u, v and w are the x, y and σ velocity components, respectively; t is the time; ζ is the water elevation; D is the total water depth (=H+ζ, in which H is the bottom depth); P_{atm} is the atmospheric pressure; ρ is the seawater density being a polynomial function of temperature T and salinity S (Millero & Poisson, 1981); f is the local Coriolis parameter (dependent on local latitude and the angular speed of the Earth's rotation); g is the acceleration due to gravity (=9.81 m/s^2); ρ_0 is the mean seawater density (=1025 kg/m^3); K_m and K_h are the vertical eddy viscosity coefficient and thermal vertical eddy diffusion coefficient; F_u, F_v, F_T and F_S are the horizontal u-momentum, v-momentum, thermal and salt diffusion terms, respectively; q^2 is the turbulent kinetic energy; l is the turbulent macroscale; K_{q^2} is the vertical eddy diffusion coefficient of the turbulent kinetic energy; $\widetilde{W}$ is a wall proximity function (=1+$E_2(\frac{l}{\kappa L})^2$, where the parameter $L^{-1}=(\zeta\text{-}z)^{-1}+(H+z)^{-1}$); F_{q^2} and F_{q^2l} represent the horizontal diffusion terms of turbulent kinetic energy and turbulent macroscale; and B_1, E_1 and E_2 are the empirical constants assigned as 16.6, 1.8 and 1.33, respectively.

Mode splitting technique is applied to permit the separation of 2D depth-averaged external mode and 3D internal mode, allowing the use of large time step. 3D internal mode is numerically integrated using a second-order Runge-Kutta time-stepping scheme, while 2D external mode is integrated using a modified fourth-order Runge-Kutta time-stepping scheme. A schematic solution procedure of this 3D model is illustrated in Figure 4. The point wetting/drying treatment technique is included to predict the water covering and uncovering process in the inter-tide zone. In the case of typhoon, the accuracies of the atmospheric pressure and wind fields are crucial to the simulation of storm surge. In this study, an analytical cyclone model developed by Jakobsen & Madsen (2004) is applied to predict pressure gradient and wind stress. The shape parameter and cyclonic regression parameter are determined by the formula suggested by Hubbert et al. (1991) and the available field observations in the Hangzhou Bay (Chang & Pon, 2001), respectively. Please refer to Guo et al. (2009) for more information.

3.2 Boundary conditions

The moisture flux and net heat flux can be imposed on the sea surface and bottom boundaries, but are not considered in this study. The method of Kou et al. (1996) is used to estimate the bottom shear stress induced by bottom boundary friction, accounting for the impact of flow acceleration and non-constant stress in tidal estuary. A river runoff (Q=1050 m^3/s) from the Qiantang River according to long-term field observation is applied on the land side of the model domain. The elevation clamped open boundary condition and atmospheric force (wind stress and pressure gradient) above sea surface are the main driving forces of numerical simulation. In modeling astronomical tide, the time-dependent open-sea elevations are from field observation at stations T7-T8 and zero atmospheric force is given. In modeling typhoon-induced storm surge, the time-dependent open-sea elevations are from FES2004 model (Lyard et al., 2006) and typhoon-generated water surface variations and atmospheric force is estimated by the analytical cyclone model. In this study, the external time step is Δt_E=2 sec and the ratio of internal time step to external time step is I_S=5.

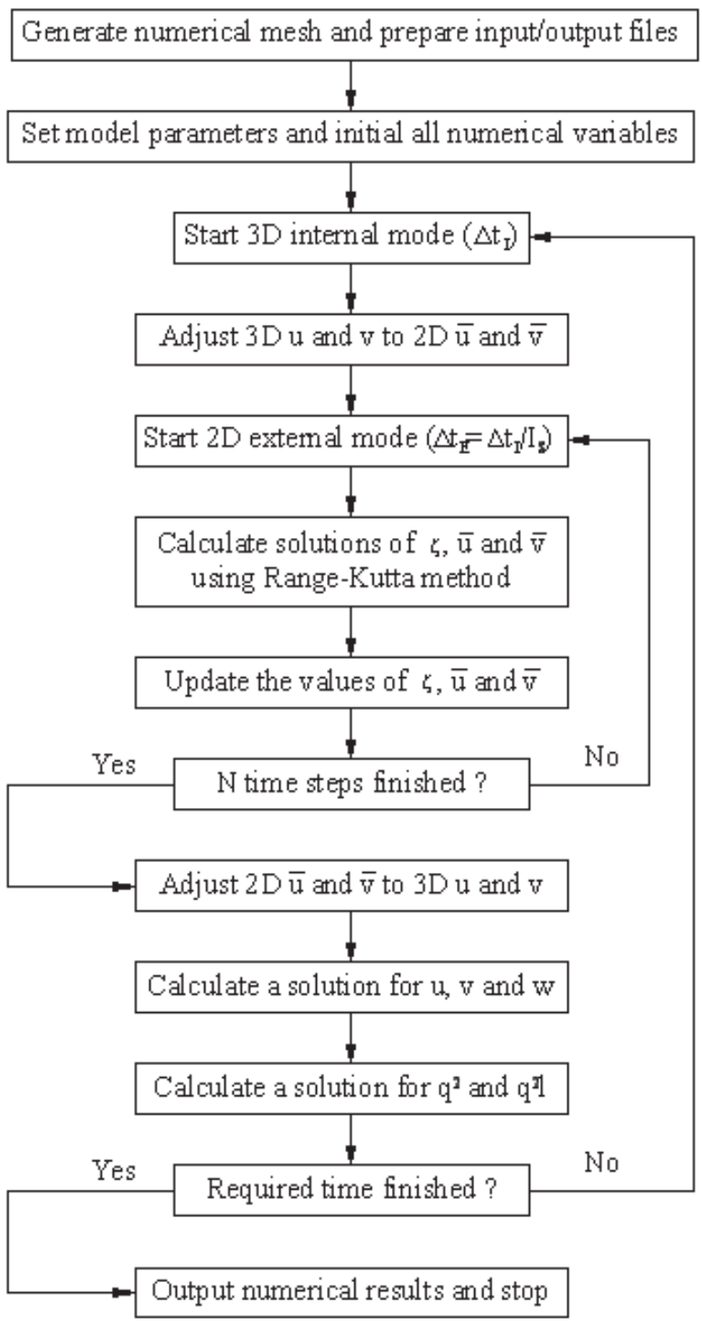

Fig. 4. A schematic solution procedure of 3D estuarine modeling

3.3 Mesh generation

As shown in Figures 1 and 2, the Hangzhou Bay has a very irregular shoreline. Therefore, to accurately represent the computational domain of the Hangzhou Bay, unstructured triangular meshes with arbitrarily spatially-dependent size were generated. The area of the whole solution domain defined for astronomical tide modeling is about 5360 km^2. The computational meshes were carefully adapted and refined, especially in the inter-tide zone, until no significant changes in the solution were achieved. The final unstructured grid having 90767 nodes and 176973 elements in the horizontal plane (each σ-level) was used with minimal distance of 20 m in the cells (see Figure 5). In the vertical direction, 11 σ-levels (10 σ-layers) compressing the σ mesh near the water surface and sea bottom symmetrically about the mid-depth are applied.

In modeling typhoon-induced storm surge, a large domain-localized grid resolution strategy is applied in mesh generation, defining very large computational domain covering the main area of typhoon and locally refining the concerned regions with very small triangular meshes. The whole computational domain covers an extensive range of 116-138°E in longitude and 21-41°N in latitude. The final unstructured grid having 111364 nodes and 217619 elements in the horizontal plane (each σ-level) was used with the minimal 100 m grid size near shoreline and the maximal 10000 m grid size in open-sea boundary (see Figure 6). In the vertical direction, 6 σ-levels (5 σ-layers) is uniformly applied.

4. Results and discussion

The results from field observation and numerical simulation are compared and further used to investigate the characteristics of tidal hydrodynamics in the Hangzhou Bay with/without the presence of typhoon.

4.1 Astronomical tide

4.1.1 Tidal elevation

Figures 7 and 8 are the comparison of simulated and observed tidal elevations at 5 stations (T2, T3, T4, T5 and T6) in spring tide and neap tide, respectively. The x-coordinate of these figures is in the unit of day, and, for example, the label '21.25 August 2005' indicates '6:00am of 21/08/2005'. Both the numerical simulation and field observation for spring and neap tides show that the tidal range increases significantly as it travels from the lower estuary (about 6.2 m in spring tide and 3.1 m in neap tide at T6) towards the middle estuary (about 8.1 m in spring tide and 3.7 m in neap tide at T4), mainly due to rapid narrowing of the estuary. The tidal range reaches the maximum at Ganpu station (T4) and decreases as it continues traveling towards the upper estuary (about 4.4 m in spring tide and 2.5 m in neap tide at T2). In general, very good agreement between the simulation and observation is obtained. There exists, however, a slight discrepancy between the computed and observed tidal elevations at T2 (Yanguan). The reason for this may be ascribed to that the numerical model does not consider the tidal bore, which may have significant effect on the tidal elevations at the upper reach. Such impact on tidal elevations, however, decreases and becomes negligible at the lower reach of the estuary.

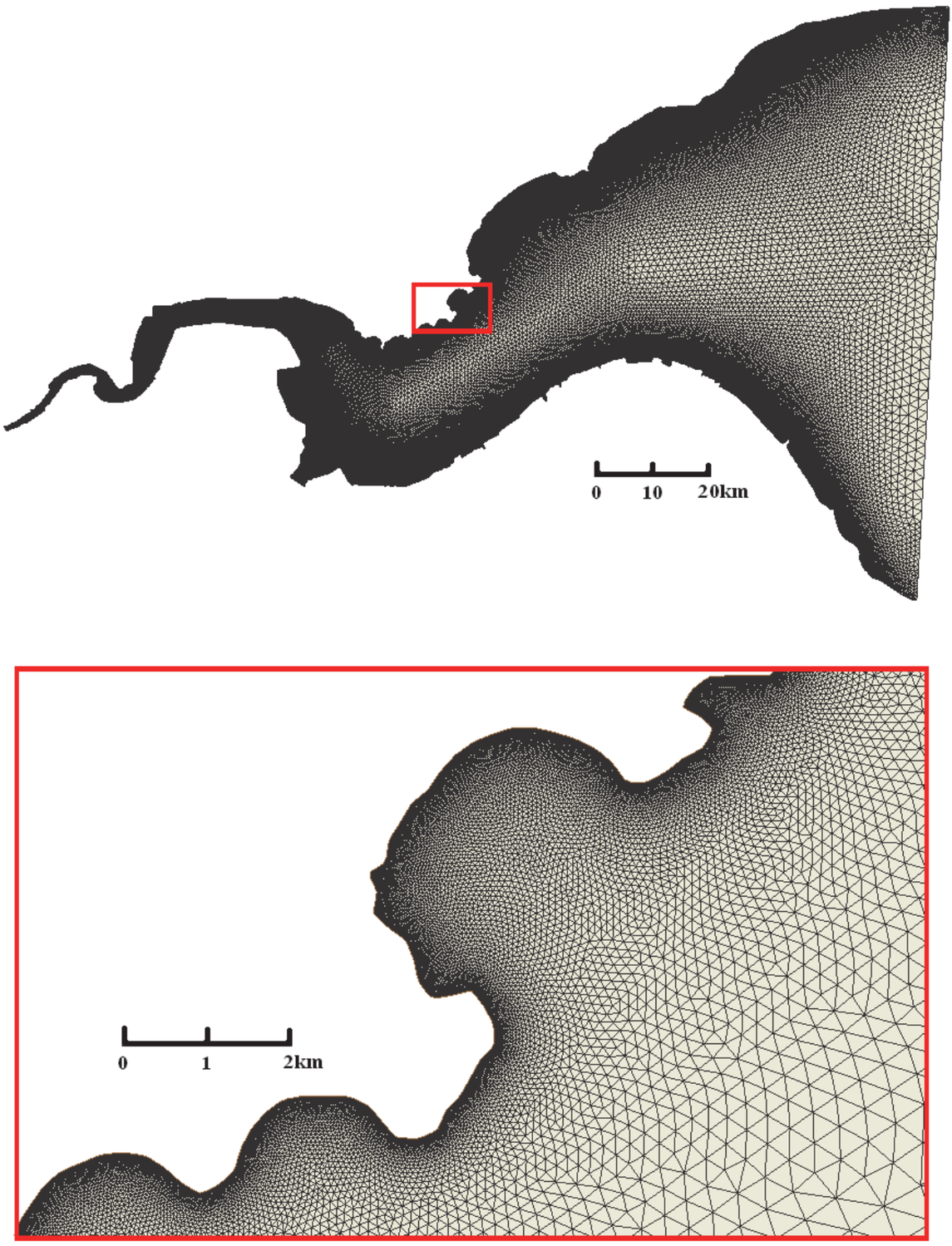

Fig. 5. A sketch of triangular grid (upper) and locally zoomed in mesh near Ganpu station (lower) for modeling astronomical tide

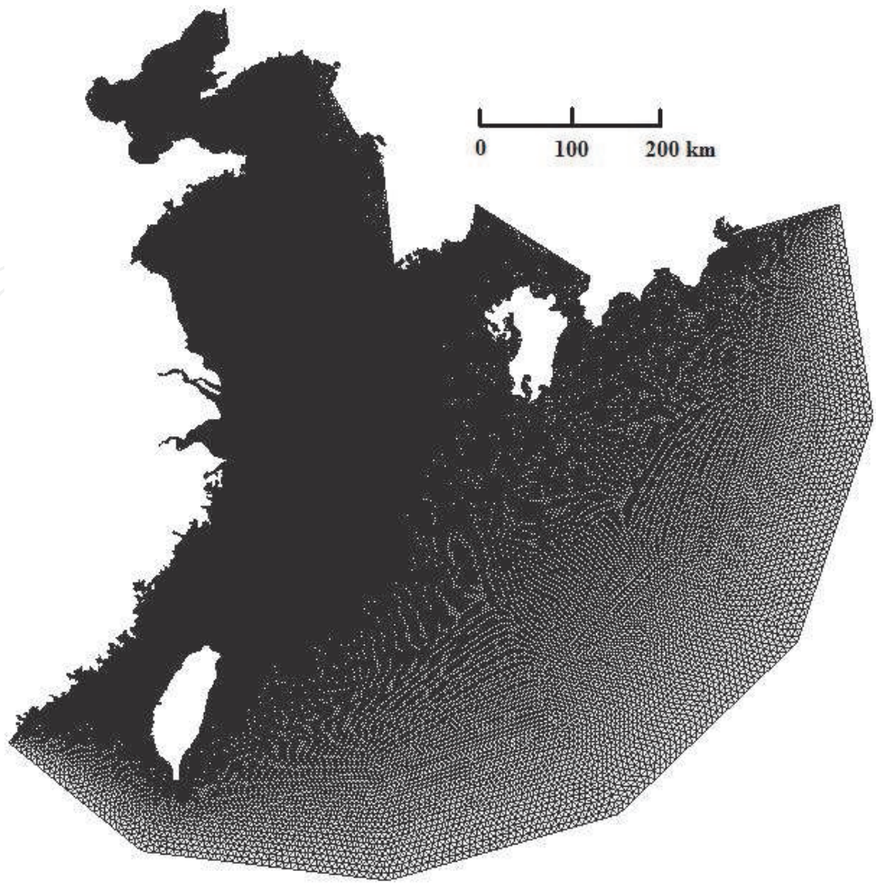

Fig. 6. A sketch of triangular grid for modeling typhoon-induced storm tide

4.1.2 Current velocity

It is clearly seen from Figures 7 and 8 that the maximum tidal ranges occur at the Ganpu station (T4). Thus, it is expected that the maximum tidal current may occur near this region. The tidal currents were measured at four locations H1-H4 across the estuary near Ganpu. These measurements are used to verify the numerical model. Figures 9 and 10 are the comparison between simulated and measured depth-averaged velocity magnitude and direction for the spring and neap tidal currents, respectively. It is seen that the flood tidal velocity is clearly greater than the ebb flow velocity for both the spring and neap tides. The maximum flood velocity occurs at H2 with the value of about 3.8 m/s, while the maximum ebb flow velocity is about 3.1 m/s during the spring tide. During the neap tide, the maximum velocities of both the flood and ebb are much less than those in the spring tide with the value of 1.5 m/s for flood and 1.2 m/s for ebb observed at H2. The maximum relative error for the ebb flow is about 17%, occurring at H2 during the spring tide. For the flood flow the maximal relative error occurs at H3 and H4 for both the spring and neap tides with values being about 20%. In general, the depth-averaged simulated velocity magnitude and current direction agree well with the measurements, and the maximal error percentage in tidal current is similar as that encountered in modeling the Mahakam Estuary (Mandang & Yanagi, 2008).

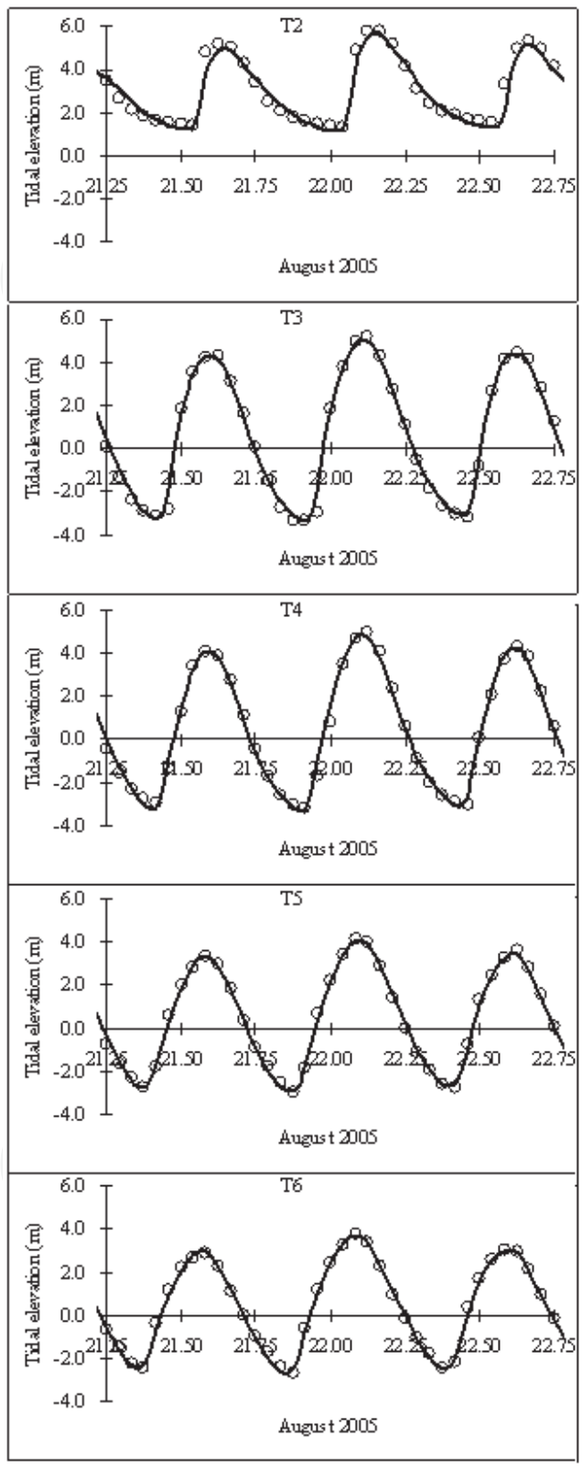

Fig. 7. Comparison of the computed and measured spring tidal elevations at stations T2-T6. −: computed; ○: measured

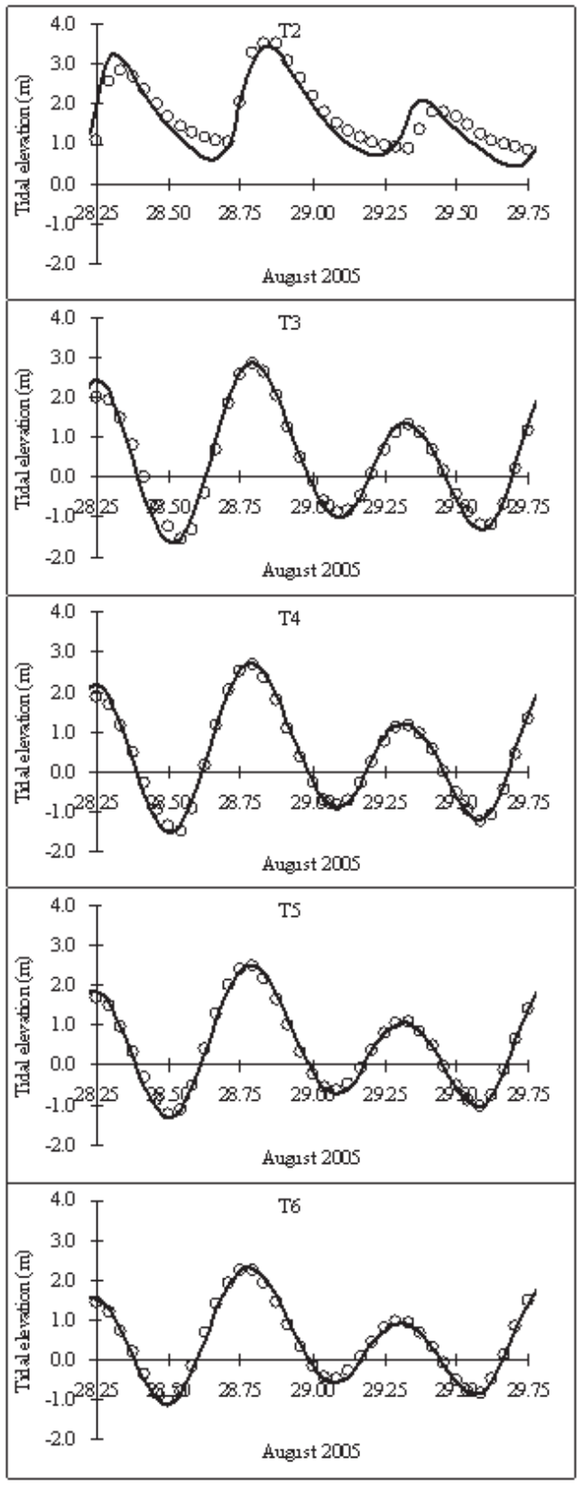

Fig. 8. Comparison of the computed and measured neap tidal elevations at stations T2-T6. —: computed; ○: measured

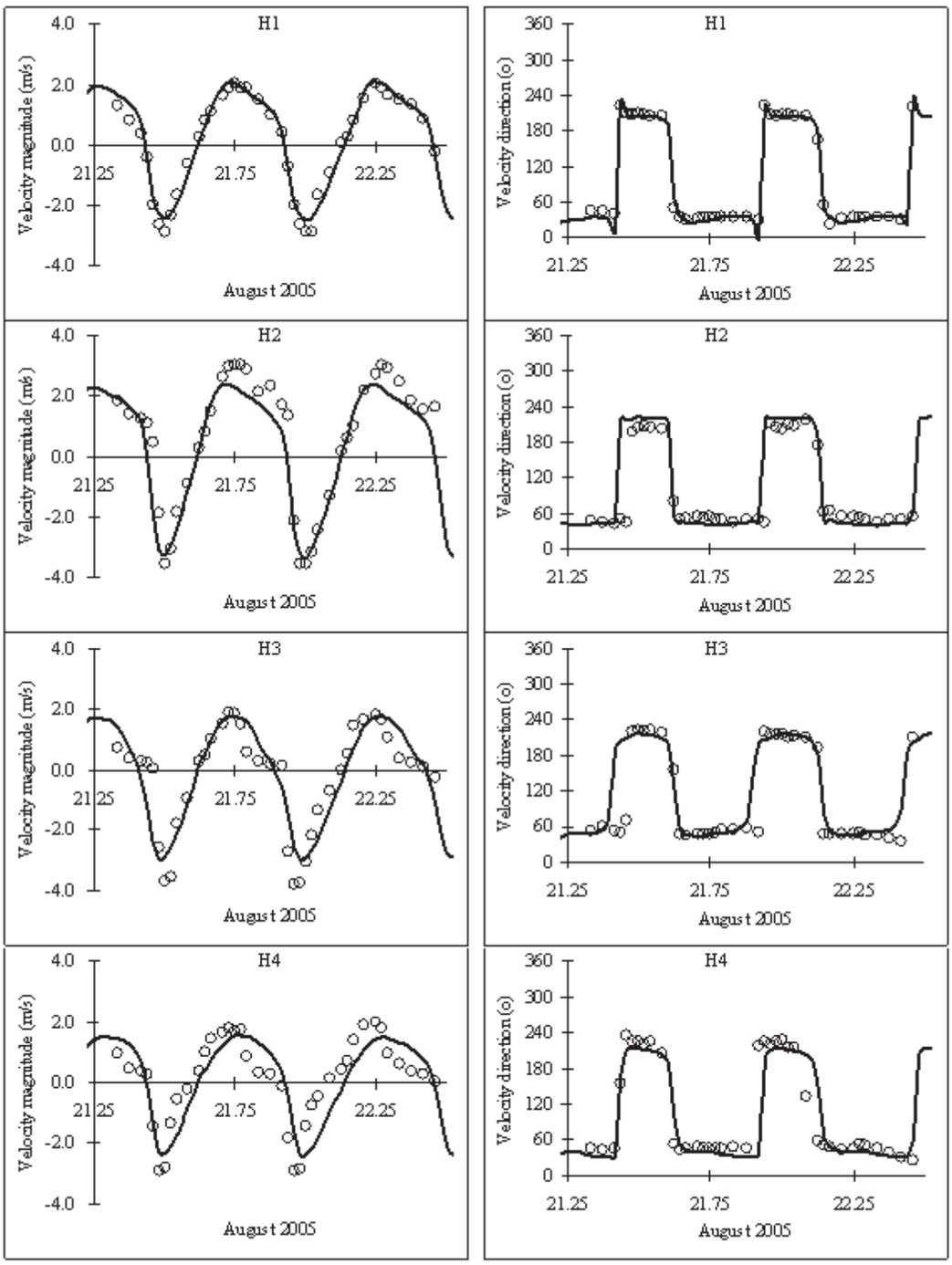

Fig. 9. Comparison of the computed and measured depth-averaged spring current velocities at stations H1-H4. —: computed; ○: measured

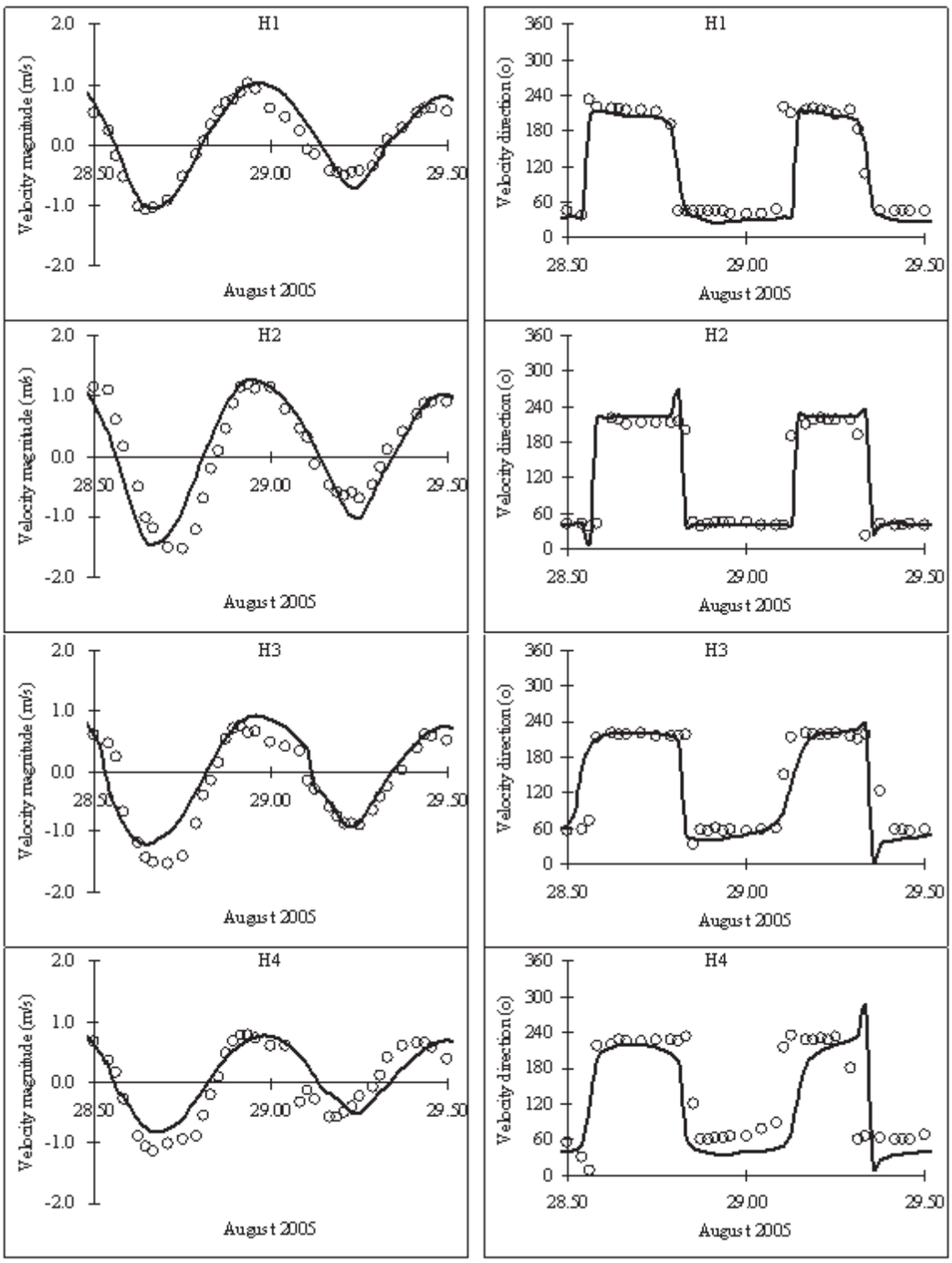

Fig. 10. Comparison of the computed and measured depth-averaged neap current velocities at stations H1-H4. —: computed; ○: measured

The vertical distributions of current velocities during spring tide are also compared at stations H1 and H4. The measured and simulated flow velocities in different depths (sea surface, 0.2D, 0.4D, 0.6D and 0.8D, where D is water depth) at these two stations are shown in Figures 11 and 12. It is noted that the current magnitude obviously decreases with a deeper depth (from sea surface to 0.8D), while the flow direction remains the same. The numerical model generally provides accurate current velocity along vertical direction, except that the simulated current magnitude is not as high as that of measured during the flood tide. The maximum relative error in velocity magnitude during spring tide is about 32% at H4 station. Analysis suggests that the errors in the tidal currents estimation are mainly due to the calculation of bottom shear stress. Although the advanced formulation accounts for the impacts of flow acceleration and non-constant stress distribution on the calculation of bottom shear stress, it can not accurately describe the changeable bed roughness that depends on the bed material and topography.

4.2 Typhoon-induced storm surge

4.2.1 Wind field

Figures 13 and 14 show the comparisons of calculated and measured wind fields at Daji station and Tanxu station during Typhoon Agnes, in which the starting times of x-coordinate are both at 18:00 of 29/08/1981 (Beijing Mean Time). In general, the predicted wind directions agree fairly well with the available measurement. However, it can be seen that calculated wind speeds at these two stations are obviously smaller than observations in the early stage of cyclonic development and then slightly higher than observations in later development. The averaged differences between calculated and observed wind speeds are 2.6 m/s at Daji station and 2.1 m/s at Tanxu station during Typhoon Agnes. This discrepancy in wind speed is due to that the symmetrical cyclonic model applied does not reflect the asymmetrical shape of near-shore typhoon.

4.2.2 Storm surge

Figure 15 displays the comparison of simulated and measured tidal elevations at Daji station and Tanxu station, in which the starting times of x-coordinate are both at 18:00 on 29/08/1981 (Beijing Mean Time). It can be seen from Figure 15 that simulated tidal elevation of high tide is slightly smaller than measurement, which can be directly related to the discrepancy of calculated wind field (shown in Figures 13 and 14). A series of time-dependent surge setup, the difference of tidal elevations in the storm surge modeling and those in purely astronomical tide simulation, are used to represent the impact of typhoon-generated storm. Figure 16 having a same starting time in x-coordinate displays simulated surge setup in Daji station and Tanxu station. There is a similar trend in surge setup development at these two stations. The surge setup steadily increases in the early stage (0-50 hour) of typhoon development, and then it reaches a peak (about 1.0 m higher than astronomical tide) on 52nd hour (at 22:00 on 31/08/1981). The surge setup quickly decreases when the wind direction changes from north-east to north-west after 54 hour. In general, the north-east wind pushing water into the Hangzhou Bay significantly leads to higher tidal elevation, and the north-west wind dragging water out of the Hangzhou Bay clearly results in lower tidal elevation. The results indicate that the typhoon-induced external forcing, especially wind stress, has a significant impact on the local hydrodynamics.

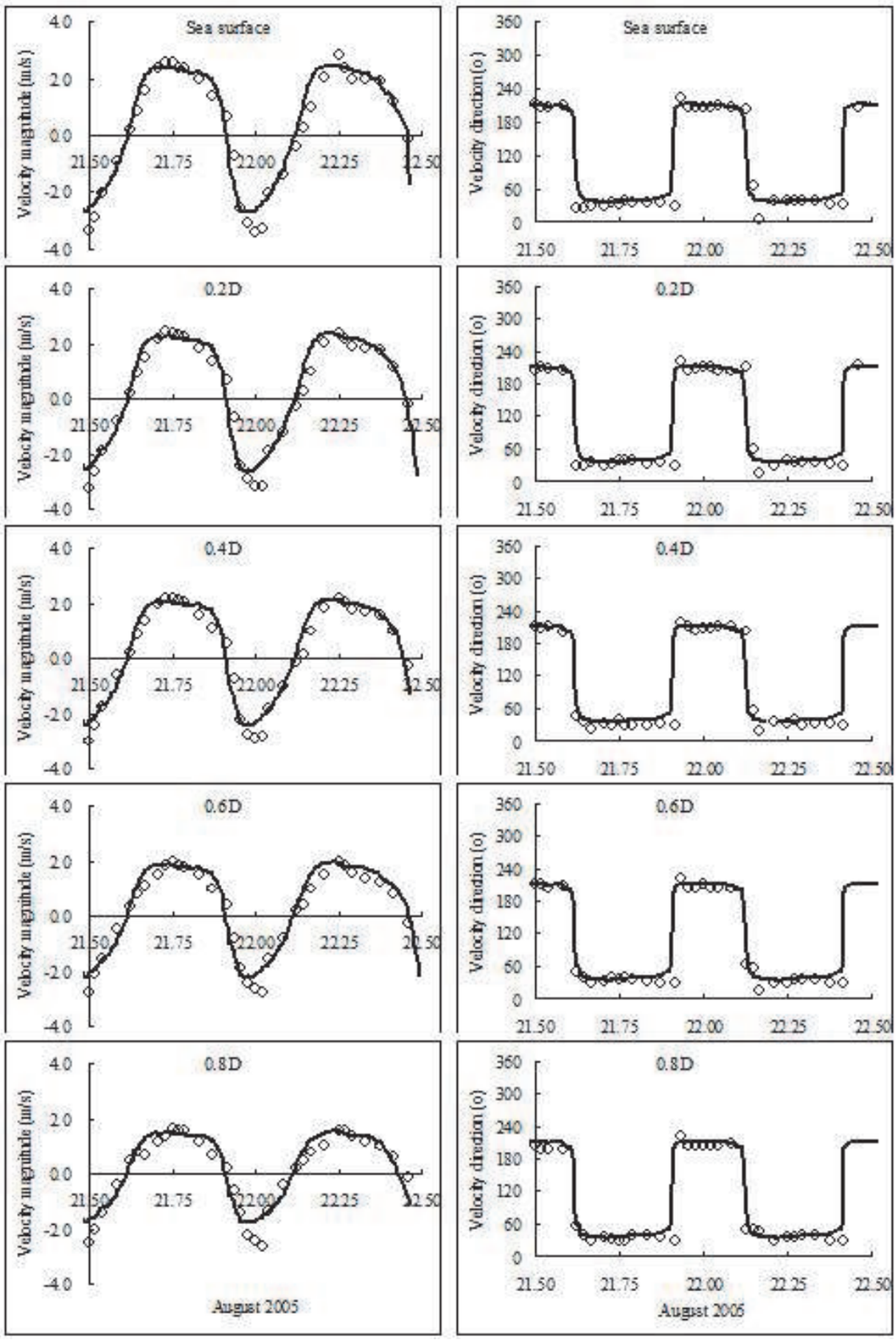

Fig. 11. Comparison of the computed and measured spring current velocities at different depths at station H1. —: computed; ○: measured

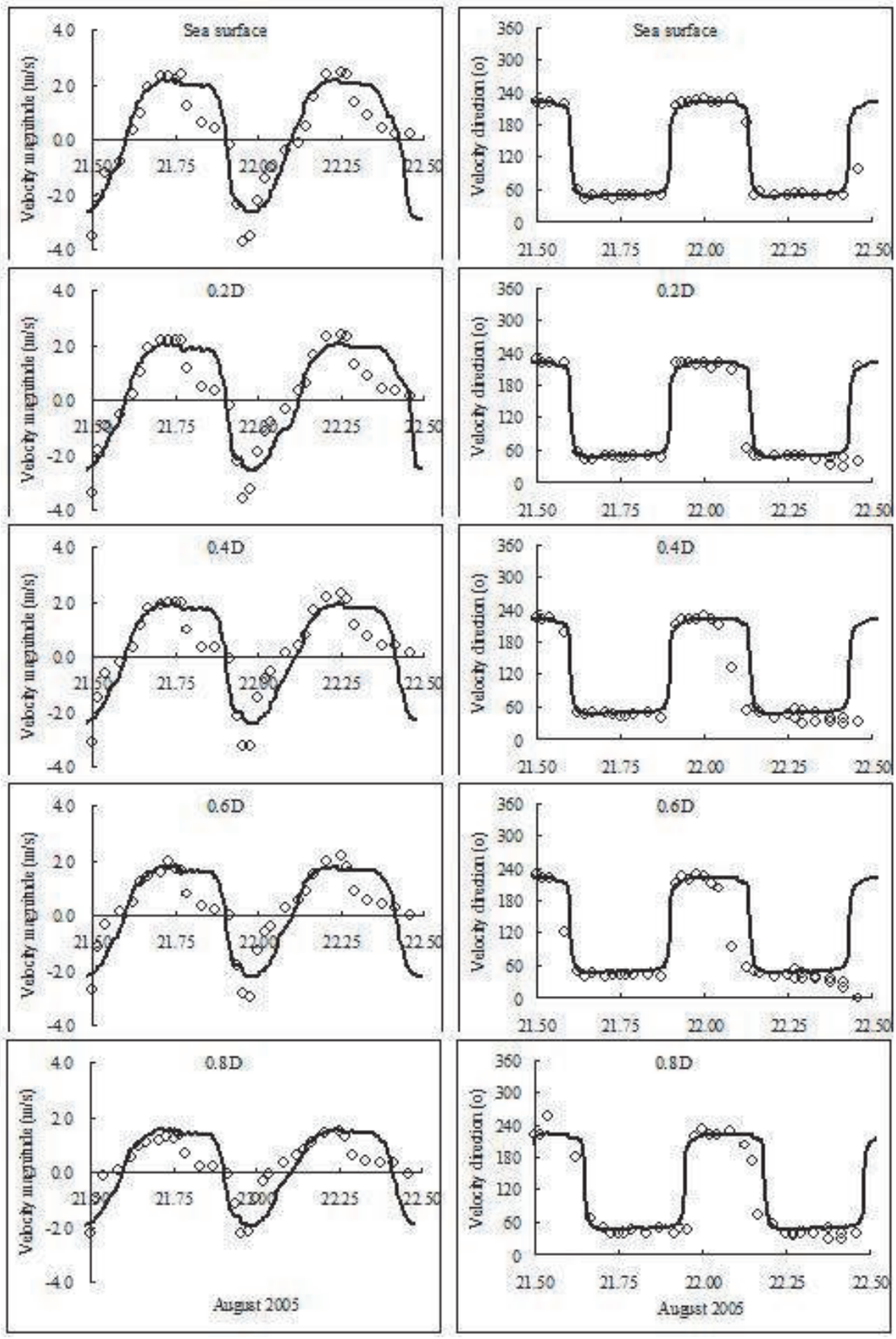

Fig. 12. Comparison of the computed and measured spring current velocities at different depths at station H4. —: computed; ○: measured

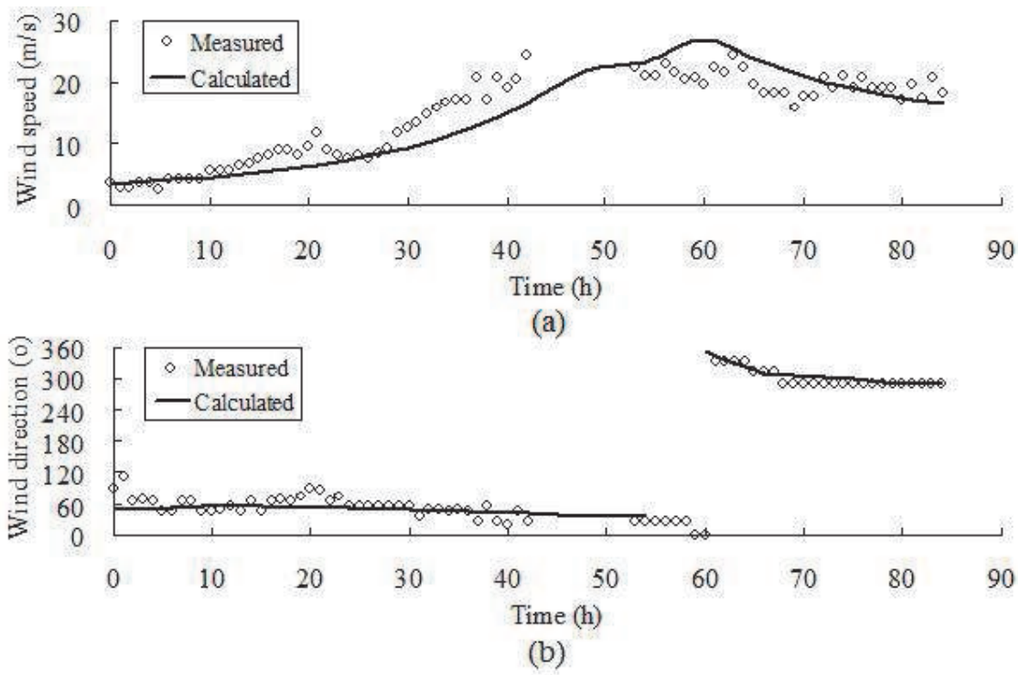

Fig. 13. Comparison of calculated and measured wind fields at Daji station during Typhoon Agnes. (a): wind speed; (b): wind direction. Starting time 0 is at 18:00 of 29/08/1981

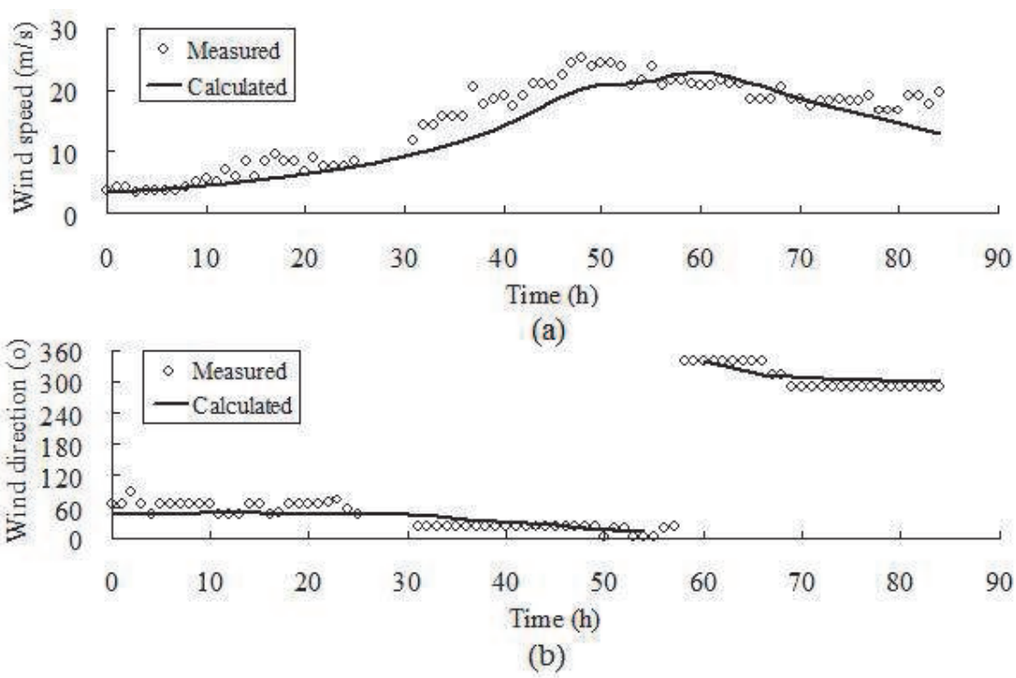

Fig. 14. Comparison of calculated and measured wind fields at Tanxu station during Typhoon Agnes. (a): wind speed; (b): wind direction. Starting time 0 is at 18:00 of 29/08/1981

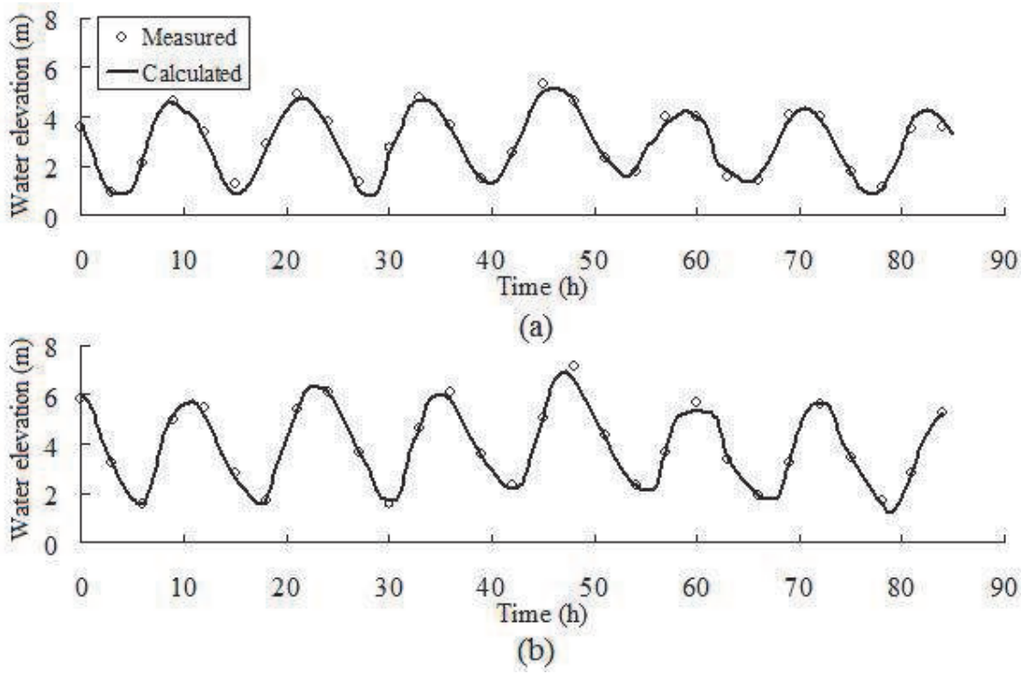

Fig. 15. Comparison of calculated and measured water elevations during Typhoon Agnes. (a): Daji station; (b): Tanxu station. Starting time 0 is at 18:00 of 29/08/1981

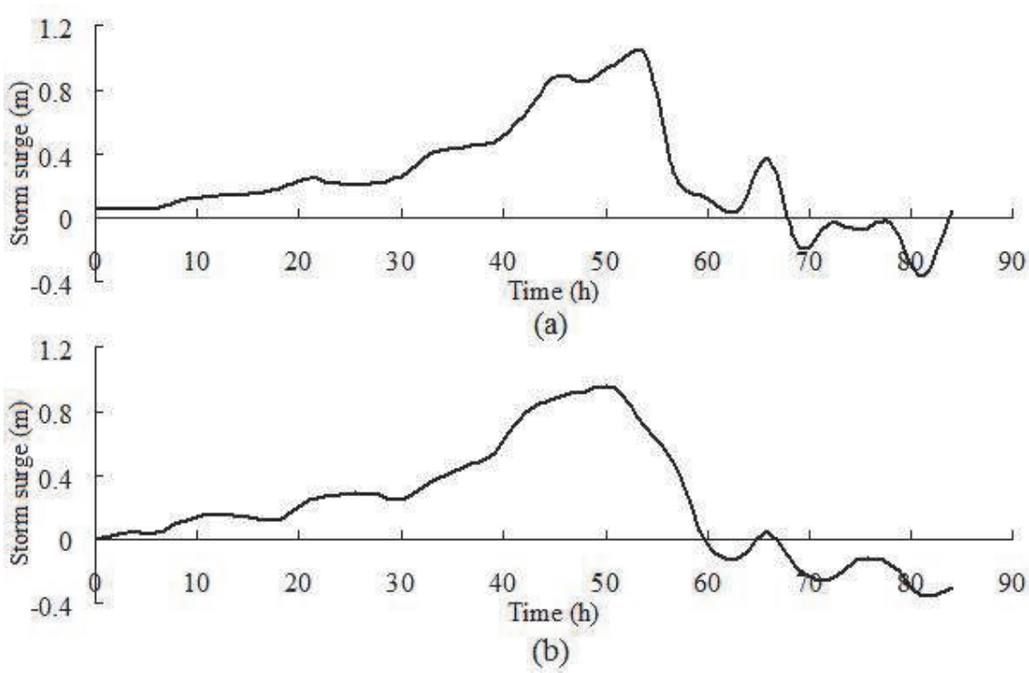

Fig. 16. The simulated surge setup at two stations during Typhoon Agnes. (a) Daji station; (b) Tanxu station. Starting time 0 is at 18:00 of 29/08/1981

5. Conclusions

In this study, the results from field observation and 3D numerical simulation are used to investigate the characteristics of astronomical tide and typhoon-induced storm surge in the Hangzhou Bay. Some conclusions can be drawn as below:

1. Tidal hydrodynamics in the Hangzhou Bay is significantly affected by the irregular geometrical shape and shallow depth and is mainly controlled by the M_2 harmonic constituent. The presence of tropical typhoon makes the tidal hydrodynamics in the Hangzhou Bay further complicated.
2. The tidal range increases significantly as it travels from the lower estuary towards the middle estuary, mainly due to rapid narrowing of the estuary. The tidal range reaches the maximum at Ganpu station (T4) and decreases as it continues traveling towards the upper estuary.
3. The flood tidal velocity is clearly greater than the ebb flow velocity for both the spring and neap tides. The maximum flood velocity occurs at H2 with the value of about 3.8 m/s, while the maximum ebb flow velocity is about 3.1 m/s during the spring tide. During the neap tide, the maximum velocities of both the flood and ebb are much less than those in the spring tide with the value of 1.5 m/s for flood and 1.2 m/s for ebb observed at H2.
4. The vertical distributions of current velocity at stations H1 and H4 show that the current magnitude obviously decreases with a deeper depth (from sea surface to 0.8D), while the flow direction remains the same.
5. Tropical cyclone, in terms of wind stress and pressure gradient, has a significant impact on its induced storm surge. In general, the north-east wind pushing water into the Hangzhou Bay significantly leads to higher tidal elevation, and the north-west wind dragging water out of the Hangzhou Bay clearly results in lower tidal elevation.

6. References

Cao, Y. & Zhu, J. "Numerical simulation of effects on storm-induced water level after contraction in Qiantang estuary," *Journal of Hangzhou Institute of Applied Engineering*, vol. 12, pp. 24-29, 2000.

Chang, H. & Pon, Y. "Extreme statistics for minimum central pressure and maximal wind velocity of typhoons passing around Taiwan," *Ocean Engineering*, vol. 1, pp. 55-70, 2001.

Chen, C., Liu, H. & Beardsley, R. "An unstructured, finite-volume, three-dimensional, primitive equation ocean model: application to coastal ocean and estuaries," *Journal of Atmospheric and Oceanic Technology*, vol. 20, pp. 159-186, 2003.

Guo, Y., Zhang, J., Zhang, L. & Shen, Y. "Computational investigation of typhoon-induced storm surge in Hangzhou Bay, China," *Estuarine, Coastal and Shelf Science*, vol. 85, pp. 530-536, 2009.

Hu, K., Ding, P., Zhu, S. & Cao, Z. "2-D current field numerical simulation integrating Yangtze Estuary with Hangzhou Bay," *China Ocean Engineering*, vol. 14(1), pp. 89-102, 2000.

Hu, K., Ding, P. & Ge, J. "Modeling of storm surge in the coastal water of Yangtze Estuary and Hangzhou Bay, China," *Journal of Coastal Research*, vol. 51, pp. 961-965, 2007.

Hubbert, G., Holland, G., Leslie, L. & Manton, M. "A real-time system for forecasting tropical cyclone storm surges," *Weather Forecast*, vol. 6, pp. 86-97, 1991.

Jakobsen, F. & Madsen, H. "Comparison and further development of parametric tropic cyclone models for storm surge modeling," *Journal of Wind Engineering and Industrial Aerodynamics*, vol. 92, pp. 375-391, 2004.

Kou, A., Shen, J. & Hamrick, J. "Effect of acceleration on bottom shear stress in tidal estuaries," *Journal of Waterway, Port, Coastal and Ocean Engineering*, vol. 122, pp. 75-83, 1996.

Lyard, F., Lefevre, F., Letellier, T. & Francis, O. "Modelling the global ocean tides: modern insights from FES2004," *Ocean Dynamics*, vol. 56, pp. 394-415, 2006.

Mandang, I. & Yanagi, T. "Tide and tidal current in the Mahakam estuary, east Kalimantan, Indonesia," *Coastal Marine Science*, vol. 32, pp. 1-8, 2008.

Mellor, G. & Yamada, T. "Development of a turbulence closure model for geophysical fluid problems," *Reviews of Geophysics and Space Physics*, vol. 20, pp. 851-875, 1982.

Millero, F. & Poisson, A. "International one-atmosphere equation of seawater," *Deep Sea Research Part A*, vol. 28, pp. 625-629, 1981.

Pan, C., Lin, B. & Mao, X. "Case study: Numerical modeling of the tidal bore on the Qiantang River, China," *Journal of Hydraulic Engineering*, vol. 113(2), pp. 130-138, 2007.

Su, M., Xu, X., Zhu, J. & Hon, Y. "Numerical simulation of tidal bore in Hangzhou Gulf and Qiantangjiang," *International Journal for Numerical Methods in Fluids*, vol. 36(2), pp. 205-247, 2001.

Wang, C. "Real-time modeling and rendering of tidal in Qiantang Estuary," *International Journal of CAD/CAM*, vol. 9, pp. 79-83, 2009.

Xie, Y., Huang, S., Wang, R. & Zhao, X. "Numerical simulation of effects of reclamation in Qiantang Estuary on storm surge at Hangzhou Bay," *The Ocean Engineering*, vol. 25(3), pp. 61-67, 2007.

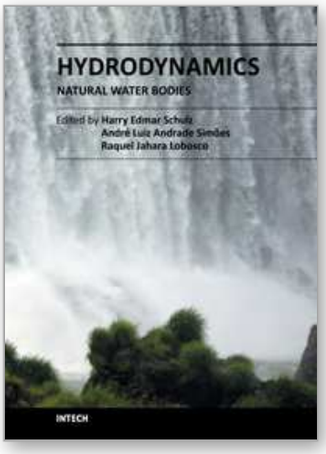

Hydrodynamics - Natural Water Bodies

Edited by Prof. Harry Schulz

ISBN 978-953-307-893-9

Hard cover, 286 pages

Publisher InTech

Published online 05, January, 2012

Published in print edition January, 2012

The knowledge of the characteristics of the fluids and their ability to transport substances and physical properties is relevant for us. However, the quantification of the movements of fluids is a complex task, and when considering natural flows, occurring in large scales (rivers, lakes, oceans), this complexity is evidenced. This book presents conclusions about different aspects of flows in natural water bodies, such as the evolution of plumes, the transport of sediments, air-water mixtures, among others. It contains thirteen chapters, organized in four sections: Tidal and Wave Dynamics: Rivers, Lakes and Reservoirs, Tidal and Wave Dynamics: Seas and Oceans, Tidal and Wave Dynamics: Estuaries and Bays, and Multiphase Phenomena: Air-Water Flows and Sediments. The chapters present conceptual arguments, experimental and numerical results, showing practical applications of the methods and tools of Hydrodynamics.

How to reference

In order to correctly reference this scholarly work, feel free to copy and paste the following:

Jisheng Zhang, Chi Zhang, XiuguangWu and Yakun Guo (2012). Astronomical Tide and Typhoon-Induced Storm Surge in Hangzhou Bay, China, Hydrodynamics - Natural Water Bodies, Prof. Harry Schulz (Ed.), ISBN: 978-953-307-893-9, InTech, Available from: http://www.intechopen.com/books/hydrodynamics-natural-water-bodies/astronomical-tide-and-typhoon-induced-storm-surge-in-hangzhou-bay-china

INTECH
open science | open minds

InTech Europe
University Campus STeP Ri
Slavka Krautzeka 83/A
51000 Rijeka, Croatia
Phone: +385 (51) 770 447
Fax: +385 (51) 686 166
www.intechopen.com

InTech China
Unit 405, Office Block, Hotel Equatorial Shanghai
No.65, Yan An Road (West), Shanghai, 200040, China
中国上海市延安西路65号上海国际贵都大饭店办公楼405单元
Phone: +86-21-62489820
Fax: +86-21-62489821